JOURNAL OF SOLID STATE CHEMISTRY 93, 53–62 (1991)

RF–Microwave Dielectric Relaxations and Frequency-Dependent Conductivity in β-$Na_{0.33}V_2O_5$ Bronze Obtained by the Sol–Gel Process

J. C. BADOT AND N. BAFFIER

Laboratoire de Chimie Appliquée de l'Etat Solide, URA 302 CNRS, ENSCP, 11 rue P. et M. Curie, 75231 Paris Cédex 05, France

Received November 13, 1990; in revised form February 21, 1991

The results concerning the complex dielectric permittivity and frequency-dependent conductivity in a broad frequency range, 10^6–10^{10} Hz, of monoclinic bronze β-$Na_{0.33}V_2O_5$ synthesized by the sol–gel process between 240 and 300 K are presented. The dielectric and conductivity spectra were performed along the direction parallel to the c-axis of the bronze structure. Two relaxations are observed and assigned to the Na^+ cation and electron hopping. Relaxation times and electronic conductivity mechanisms are discussed. © 1991 Academic Press, Inc.

Introduction

β-$Na_{0.33}V_2O_5$ bronze (Fig. 1) has been synthesized by the sol–gel process by a heat treatment of the vanadium oxide xerogel $Na_{0.33}V_2O_5$-$1.6H_2O$ (*1*). Compared with the classical synthesis of a mixture of oxides, this type of synthesis offers specific advantages for the formation of fibers or films, particularly in the case of low-dimensional solids built from stacking of sheets or juxtaposition of fibers. In this latter case, the sol–gel process increases the anisotropy of the initial material (*1*). In this way, the sodium vanadium bronze is obtained as a thin layer or a film. It has been shown that the electrochemical properties of this material were much improved and that it could be considered as a very good material for secondary lithium batteries (*2*).

This bronze obtained by the sol–gel process (hereafter referred to as SGP bronze) has the same monoclinic structure (a = 10.10 Å, b = 3.63 Å, c = 15.15 Å, β = 110°) as the usual bronze obtained through solid state reaction at 650°C (hereafter referred to as SSR bronze). X-ray diffraction patterns of SGP bronze have shown a preferred orientation of the film parallel to the *ab*-plane, i.e., perpendicular to the c-axis. The bronze contains V^{4+} and V^{5+} ions localized on the V_1 and V_2 octahedral sites and bipyramidal V_3 sites (Fig. 1). Sodium ions are equally distributed on the sites M_1 and M_1' in the tunnels of the network made of VO_5 bipyramids linear chains (*3–5*). Galy *et al.* (*5*) have shown that this bronze structure presents two other available tunnel sites: M_3 tetrahedra and eight-coordinated M_2 sites.

In the case of SSR bronze, previous studies made on single crystals (*6, 7*) have shown that the vanadium ions are found in both V^{4+} and V^{5+} states with the formation of V^{4+}–V^{4+} pairs along zig-zag chains of V_1

0022-4596/91 $3.00

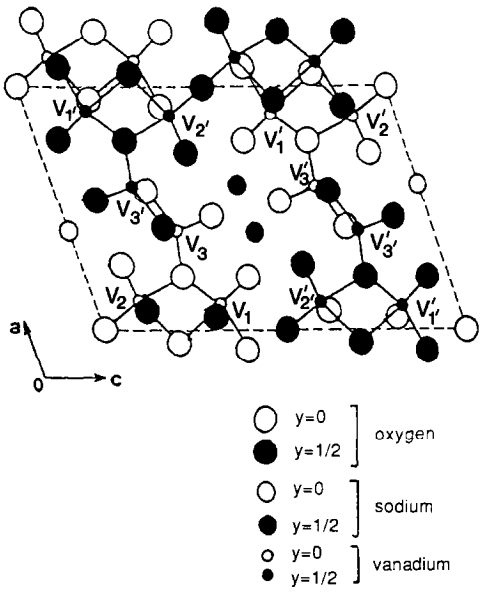

FIG. 1. Projection in the *ac*-plane of the atomic positions in the monoclinic $Na_{0.33}V_2O_5$ bronze.

sites parallel to the *b*-axis. In the bipolaron model of Chakraverty *et al.* (*8*), the V^{4+}–V^{4+} pair has a spin singlet ground state, the first excited state of the bipolaron being a triplet state. Since the "dissociation energy" 2Δ ($\Delta/k \approx 170$ K) of the bipolaron is smaller than the singlet–triplet exchange energy $2J$ (*5*), the triplet state is not accessible thermally. The bronze is a "quasi-1D" conductor, since the conductivity along the *b*-axis is somewhere between 10 and 100 S · cm^{-1} at room temperature and exceeds the conductivity in the *ac*-plane by about two orders of magnitude (*9*, *10*). The conductivity is of the semiconducting type with an activation energy of 0.05–0.08 eV. In relation to the structure and EPR measurements (*11*), the high conductivity was explained in terms of collective motion of bipolarons along the zig-zag chains parallel to the *b*-axis between V_1 sites. In the direction perpendicular to the *b*-axis, i.e., parallel to the *ac*-plane, electron hopping occurs along V_1–V_3–$V_{3'}$–$V_{1'}$ sequences.

In the case of SGP bronze powders and orientated films (*12*), we have shown previously that the electronic properties are not modified by the synthesis method and are similar to those of SSR bronze single crystals. Magnetic susceptibility and EPR measurements have evidenced that the bipolaron model of Chakraverty can be applied. Several parameters have the same value for both SSR and SGP bronzes: this is the case for the unpaired electron occupancy of the V_1 (84%) and V_3 (16%) sites and 2Δ ($\Delta/k \approx 170$ K).

The observed conductivity of SGP bronze films is also strongly anisotropic (anisotropy degree $\approx$ 200–300); the dc conductivities parallel $\sigma_\parallel$(parallel to the *ab*-plane) and perpendicular σ_c (along the *c*-axis) to the film are 8 S · cm^{-1} and 4×10^{-2} S · cm^{-1}, respectively, at room temperature with activation energy $W \approx 0.07$ eV. In a previous paper (*12*) we have shown that the conductivity $\sigma_\parallel$ parallel to the film surface is the combination of the conductivities along the *b* (σ_b) and *a* (σ_a) directions. These "*ab*" planes being oriented at random around the *c*-axis, the $\sigma_\parallel$ value can be approximated by the average value of σ_b and σ_a, i.e. $\sigma_\parallel = (\sigma_a + \sigma_b)/2$. As $\sigma_a \ll \sigma_b$ (*12*), $\sigma_\parallel \approx (\sigma_b/2)$, the conductivity parallel $\sigma_\parallel$ to the film surface corresponds essentially to the conductivity along the *b*-axis, i.e., $\sigma_b \approx 16$ S · cm^{-1} at room temperature. This result (*12*) means a collective motion of bipolarons, in the same way as in the SSR bronze single crystal (*11*).

In order to understand dynamic and transport properties of the SGP bronze, we have measured the complex conductivity and dielectric permittivity in a broad frequency range (1 MHz–10 GHz). The results are discussed and compared with those obtained on SSR bronze by EPR and NMR techniques (*11*, *13*).

Experimental

The synthesis of β-$Na_{0.33}V_2O_5$ bronze via the sol–gel process, i.e., from dehydration of vanadium oxide xerogel $Na_{0.33}V_2O_5$·1.6

H_2O, has been previously described (*1*). The sample is an oriented compacted pellet (diameter $2a = 3$ mm and thickness $d = 0.5$ to 1 mm) constituted by the superposition of several pieces of films; it is sintered at 600°C. The c-axis is perpendicular to the pellet plane. The X-ray diffraction diagram of the pellet is identical to the diagram obtained with a thin film of bronze (*1*), showing the preferential orientation of this material.

Complex permittivity $\varepsilon^*(\omega)$ and/or conductivity $\sigma^*(\omega)$ measurements have been performed, in the temperature range 240–300 K, under N_2 flux, between 1 MHz and 10 GHz using an RF impedance analyzer (Model HP4191A) and a network analyzer (Model HP8410).

The cell is a circular coaxial line whose inner conductor is interrupted by the cylindrical sample; it is loaded with a short-circuit. The electric field in the sample is parallel to the c-axis, which is common with the axis of the inner conductor (*14–16*). The knowledge of the sample impedance Z_s allows the determination of the complex dielectric permittivity $\varepsilon^*(\omega)$ (*14–17*) according to

$$Z_s = (G_s + iC_s\omega)^{-1} = -i\omega[\mu_0 d J_0(\gamma a)]/[2\pi \gamma a J_1(\gamma a)], \quad (1)$$

where $\gamma = k(\varepsilon' - i\varepsilon'')^{1/2}$, $\mu_0 = 4\pi\ 10^{-7}$ H · m^{-1}; $\varepsilon^*(\omega) = \varepsilon' - i\varepsilon''$ is the complex permittivity of the sample. J_0 and J_1 are respectively zero- and first-order Bessel functions. G_s and C_s respectively are the conductance and the capacitance of the sample.

All the dielectric spectra have been obtained from around 100 measurement points, the frequency steps being 0.2, 10, 100, and 200 MHz, respectively, in frequency ranges 1–10 MHz, 10–100 MHz, 100–1000 MHz, and 2000–10,000 MHz. The average statistical errors on ε' and ε'' measurements are 3% approximately in the whole frequency range.

Electrodes are gold-covered brass plugs, the pellets being covered with a Pt paint deposited after compaction and sintering.

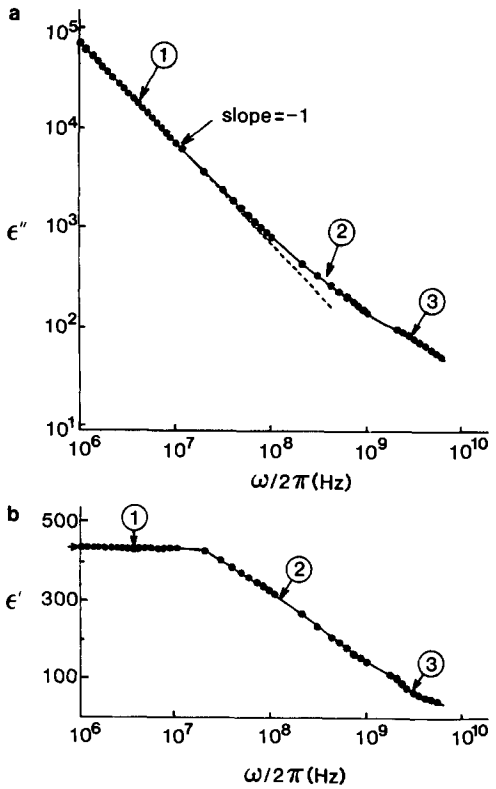

FIG. 2. Frequency dependence of (a) imaginary part $\varepsilon''(\omega)$ ("log–log" representation) and (b) real part $\varepsilon'(\omega)$ ("semi-log" representation) of the SGP bronze complex permittivity $\varepsilon^*(\omega)$ at 300 K.

Results and Discussion

Evidence of the Dielectric Relaxations

Figure 2 shows the frequency dependence between 10^6 and 10^{10} Hz of the imaginary part $\varepsilon''(\omega)$ ("log–log" representation, Fig. 2a) and of the real part $\varepsilon'(\omega)$ ("semi-log" representation, Fig. 2b) of the complex permittivity $\varepsilon^*(\omega)$.

In the low frequency part of the dielectric spectra ($10^6 \leq \omega/2\pi \leq 10^7$Hz), the frequency dependence of the loss factor $\varepsilon''(\omega)$ is a straight line whose slope is -1. Such behavior corresponds to dielectric losses ε''_{dc} due to dc conductivity σ_{dc}, i.e., $\varepsilon''_{dc} \propto (\sigma_{dc} \cdot \omega^{-1})$: for example at room temperature, $\sigma_{dc} \approx 4 \times 10^{-2}$ S · cm^{-1}. The corresponding real

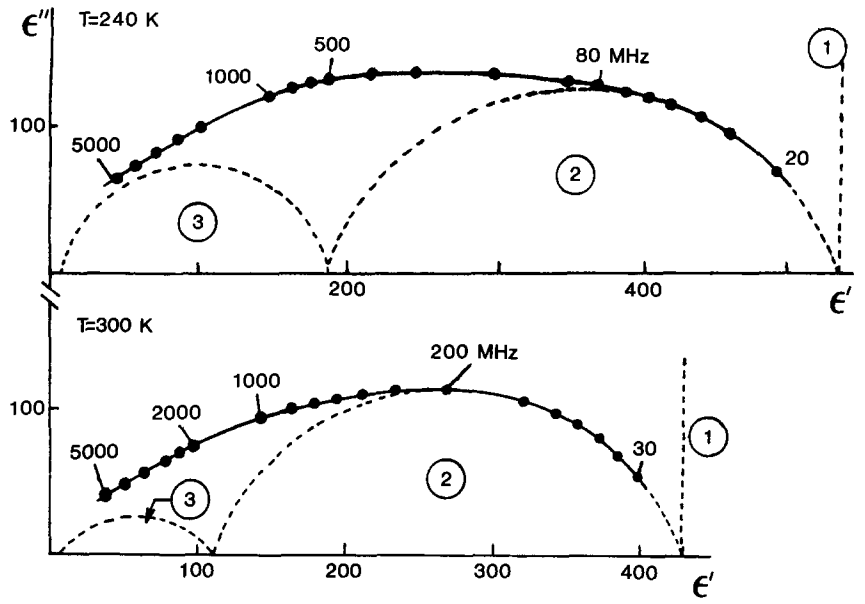

FIG. 3. Cole–Cole plots of imaginary part $\varepsilon''(\omega)$ vs real part $\varepsilon'(\omega)$ of the complex dielectric permittivity $\varepsilon^*(\omega)$ for SGP bronze at 240 and 300 K. The contribution of the dc-conductivity (domain 1) has been subtracted for convenience of scale.

part $\varepsilon'(\omega)$ is almost constant and equal to the static permittivity ε_s of the compound: for example at room temperature, $\varepsilon_s \approx 420$.

In the high frequency part of the dielectric spectra ($10^7 \leq \omega/2\pi \leq 10^{10}$Hz), Fig. 2b shows two kinks corresponding to two dielectric relaxations: one is strong between 10^7 and 10^8 Hz and the other is smaller above 10^9 Hz. The corresponding loss factor $\varepsilon''(\omega)$ presents one departure of the linear dependence and two kinks smoothed by dc-conductivity losses ε''_{dc} (Fig. 2a).

As the hypothetic relaxation domains are not well defined in direct representation (cf. Fig. 2), it is more convenient to study the evolution of the permittivity by the Cole–Cole plots method, i.e., imaginary part ε'' versus real part ε' of the dielectric permittivity $\varepsilon^*(\omega)$ (cf. Fig. 3). The decomposition of these plots shows three kinds of behaviors: one is represented by a straight line (domain 1) and the others by circular arcs (domains 2 and 3). The contribution of the dc conductivity σ_{dc} (cf. Fig. 3) has been subtracted for scale conveniences owing to the strong values of dielectric losses ε'' in comparison to those of the real part ε' for the low frequency part of the spectra (cf. Fig. 2). The decomposition procedure of the Cole–Cole plots has been already described in Ref. (*14*). The decomposition of the Cole–Cole plots into two circles is unambiguous and constitutes the best fit within the accuracy of the measurements. However, it is not possible to observe small dielectric relaxations, whose intensities are negligible compared with those of the domains 2 and 3 and lower than the apparatus resolution.

Description of the Relaxation Domains

Domain 1. This domain occurs in the low-frequency part of the spectra and is represented by a straight line perpendicular to ε'-axis. This domain corresponds to dielectric losses ε'' due to dc conductivity along the c-axis with $\varepsilon' = \varepsilon_s$ (cf. Fig. 2). The results σ_{dc}

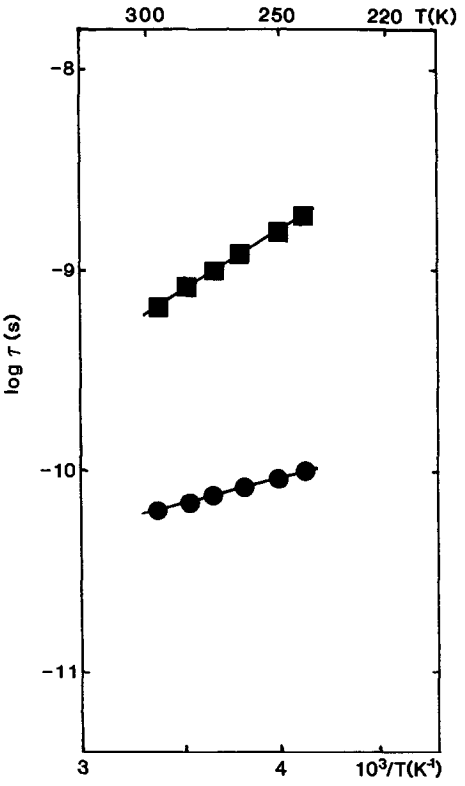

FIG. 4. Inverse temperature dependence of dielectric relaxation times τ corresponding to domains 2 (■) and 3 (cs).

$= 4.10^{-2}$ S · cm^{-1}at 300 K with activation energy $W_c = 0.07$ eV are the same as those determined on SGP bronze thin films (*10*).

Domains 2 and 3. These domains are represented by circular arcs characterizing non-Debye dielectric relaxations in RF and microwave frequencies. These behaviors (*18*) can be expressed by

$$\varepsilon^*(\omega) = \varepsilon_\infty + [\varepsilon_s - \varepsilon_\infty]/[1 + (i\omega\tau)^\beta], \quad (2)$$

where ε_∞ and ε_s are limit values of $\varepsilon^*(\omega)$, in each domain, as ω approaches ∞ and 0, respectively. The value τ is known as the (Debye) relaxation time deduced from the loss-peak frequency $f_p = (2\pi\tau)^{-1}$.

The relaxation time τ is a measure of the characteristic time scale associated with charge carriers hopping or molecular reorientation. The temperature dependence of the dielectric relaxation times τ corresponding to domains 2 and 3 follows an Arrhenius law (cf. Fig. 4), i.e., $\tau = \tau_0 \exp(W/kT)$. The experimental values are $\tau_0 = 5.10^{-12}$ sec, $W = 0.12$ eV for domain 2 and $\tau_0 = 10^{-11}$ sec, $W = 0.05$ eV for domain 3.

β is an empirical parameter which measures the "degree of departure" from the Debye model ($0 \leq \beta \leq 1$), the Debye model corresponding to $\beta = 1$. Figure 5 shows the temperature dependence of the β parameter corresponding to relaxation domains 2 and 3. The β parameter of domain 2 is almost constant, i.e., $0.7 \leq \beta \leq 0.75$, between 240 and 300 K. However, there is a strong temperature dependence for the β parameter of domain 3; it decreases with the temperature, i.e., $\beta = 0.6$ at 300 K and 0.85 at 240 K (cf. Fig. 5).

The quantity $\Delta\varepsilon = \varepsilon_s - \varepsilon_\infty$ represents the orientational electric susceptibility of each relaxation domain. Figure 6 shows that the temperature dependence of the inverse susceptibility $(\Delta\varepsilon)^{-1}$of the relaxation domains 2 and 3 is a straight line which passes through the origin. Consequently, $\Delta\varepsilon$ follows the classical law, $\Delta\varepsilon = C/T$: $C = 10^5$ K and $C = 3.10^4$ K for the relaxation domains 2 and 3, respectively.

The ε_∞ value, i.e., $\varepsilon_\infty = 10$ (cf. Fig. 3),

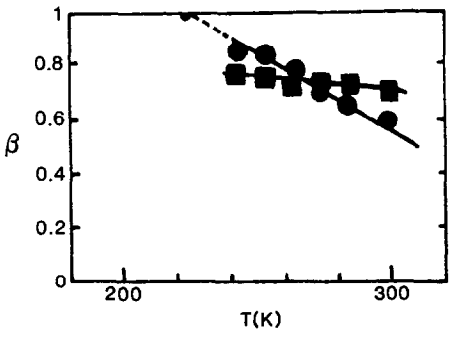

FIG. 5. Temperature dependence of β parameters corresponding to domains 2 (■) and 3 (●).

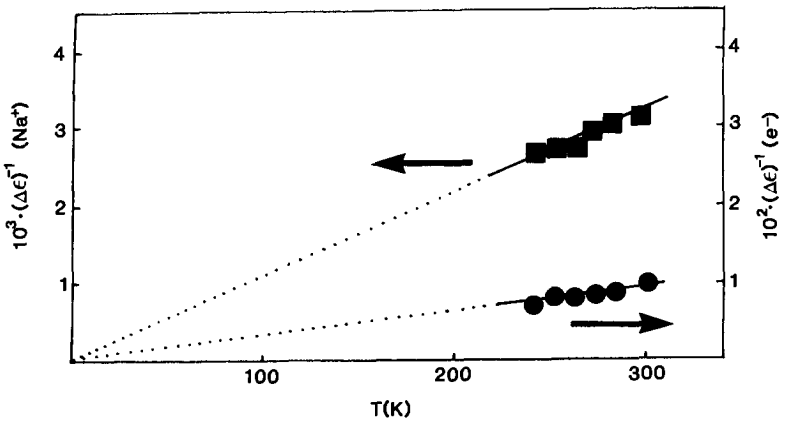

FIG. 6. Temperature dependence of inverse dielectric susceptibility $(\Delta\varepsilon)^{-1}$ for each relaxation domain (■, domain 2; ●, domain 3).

determined by extrapolation of the circular arc of domain 3 at high frequency agrees closely with the permittivity value of the pure vanadium oxide V_2O_5, $\varepsilon' = 10$ (*16*). This high value perhaps suggests the presence of other absorption bands at higher frequencies and/or relevant contributions in the far-infrared region.

Assignment of the Relaxations

The first problem to solve is the assignment of each relaxation in relation to its characteristic time, τ, activation energy, W, and dielectric susceptibility, $\Delta\varepsilon$ ($\Delta\varepsilon = \varepsilon_s - \varepsilon_\infty$). One criterion is to enumerate the species which can move in the material, i.e., polar molecules and/or charge carriers. Another criterion is the comparison of our experimental values with those obtained by other spectroscopic techniques (e.g., NMR, EPR, . . .) on the same and/or equivalent materials.

Since the β-$Na_{0.33}V_2O_5$ bronze does not contain polar molecules, only Na^+ cations in tunnels and electrons between vanadium sites can move and could eventually involve dielectric relaxations in RF and microwave regions.

In the case of SSR bronze single crystals, EPR spectroscopy (*11*) has shown that the correlation time for electron hopping $\tau_c \approx 10^{-11}$ sec, determined from linewidth measurements, is assumed to be temperature independent. The value τ_c has been considered as the hopping time between V_1 sites along the *b*-axis and between V_1 and V_3 sites in the *ac*-plane (cf. Figs. 1 and 7).

In the same material, ^{23}Na NMR studies (*13*) have evidenced Na^+ hopping in the tun-

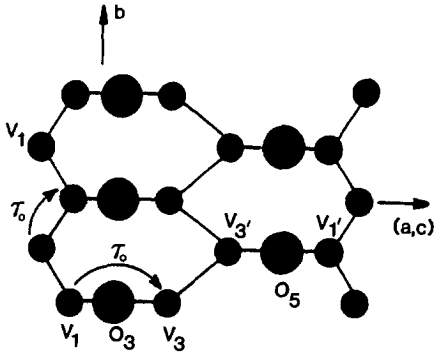

FIG. 7. Schematic representation of the electron hopping process perpendicular to the *b*-axis (τ_c corresponds to the characteristic time of electron hopping between V_1 and V_3 sites).

nels. This motion is defined by a hopping time, $\tau = \tau_0 \exp(W/kT)$, with activation energy $W = 0.15$ eV and $\tau_0 \approx 2.10^{-12}$ sec.

When we compare the characteristic time $\tau_0 \approx 5.10^{-12}$ sec and activation energy $W \approx 0.12$ eV of domain 2 with those obtained by the NMR technique, it seems reasonable to assign relaxation domain 2 to Na^+ hopping in the tunnels along the c-axis.

In comparison with the EPR study, relaxation domain 3 is due to electron hopping along the c direction, i.e., projection of the V_1–V_3–$V_{3'}$–$V_{1'}$ sequence on the c-axis (cf. Fig. 7). Actually, the characteristic time $\tau_0 \approx 10^{-11}$ sec (preexponential factor of the dielectric relaxation time $\tau = \tau_0 \exp(W/kT)$), which we have measured, corresponds to the correlation time τ_c between V_1 and V_3 sites determined by EPR study. According to previous papers (*6*, *11*), the activation energy $W = 0.05$ eV would correspond to the barrier between V_3 and $V_{3'}$; this value is in good agreement with those obtained from dc-conductivity measurements on SSR bronze single crystals (*6*, *9*, *10*). However, the discrepancy between activation energies of dc-conductivity ("long-range" conductivity) $W = 0.07$ eV and of electron hopping (along the V_1–V_3–$V_{3'}$–$V_{1'}$ sequence) $W = 0.05$ eV would be due to "grain" boundaries (more exactly oxide fiber boundaries) in the SGP sample (*12*).

Moreover, the knowledge of the electric susceptibility $(\Delta\varepsilon)_i = C_i/T$ allows the determination of the hopping distance (along the c-axis) l_i of the charge carriers, i.e. Na^+ ($i = 2$) and electrons ($i = 3$), through the equation

$$C_i = N_i(e\, l_i)^2/(\varepsilon_0 k) \quad (i = 2, 3), \quad (3)$$

where l_i is the hopping distance, N_i the number of moving charges, ε_0 the vacuum permittivity, and k the Boltzmann constant.

(a) In the case of electrons ($i = 3$), the concentration N_3 of single electrons (*11*, *12*) diffusing along the sequence V_1–V_3–$V_{3'}$–$V_{1'}$ in the ac-plane is expressed as

$$N_3 = N_0/6\ \{0.84 \exp(-\Delta/kT)/ [1 + \exp(-\Delta/kT)] + 0.16\}, \quad (4)$$

where N_0 is the number of vanadium ions.

Assuming that $N_0 = 2.27 \times 10^{28}$ m^{-3}, $\Delta/k = 170$ K (*12*), and $C_3 = 3 \times 10^4$ K (cf. Fig. 6), it is found from Eqs. (3) and (4) that the hopping distance $l_3 \approx 3.1$ Å. This latter value corresponds exactly to the projection of the length of the sequence V_1–V_3–$V_{3'}$–$V_{1'}$ on the c-axis (cf. Figs. 1 and 7). The dielectric relaxation time $\tau \approx 5.10^{-11}$ sec at room temperature (cf. Fig. 4) measures the electron hopping time between V_1 and V_1' sites via V_3 and $V_{3'}$ sites.

(b) In the case of Na^+ cations ($i = 2$), since $N_2 = N_0/6$ and $C_2 = 10^5$ K (cf. Fig. 6), it is found from Eq. (3) that the hopping distance is $l_2 \approx 4$ Å. This value would correspond to the projection on the c-axis of the distance ($M_{2'}$–M_2') between two M_2 sites (*5*). Consequently, the relaxation domain 2 would describe Na^+ cation local hopping in the ac-plane between available M_2 sites around equilibrium M_1 sites of the tunnels inside the oxide framework. Thus the obviousness of a local hopping for the Na^+ motions leads to a confinement of these ions into the cages formed by the VO_5 and VO_6 coordination polyhedra around V_3, V_1, V_1', and V_3' in the diagonal direction (*11*) of the ac-plane (cf. Fig. 1). These results are in good agreement with electrochemical studies (*2*), which have shown that the oxidation of Na^+ cations in SGP bronze was not possible; it involves the nonexistence of Na^+ long-range diffusion.

The dielectric relaxations assigned to Na^+ and electron hopping are "non-Debye" relaxations (cf. Fig. 3). This type of relaxation which always occurs in disordered systems (gels, glasses, . . .) is not well understood from the theoretical point of view; eventually several models and approaches have been proposed (*19*, *20*). Ac-

tually, the system cannot be characterized by a well-defined single relaxation time and the "non-Debye" relaxation most often is explained by assuming a distribution of relaxation times (*21*).

In the case of SGP bronze, Fig. 5 shows that the electron hopping relaxation (domain 3) tends toward Debye relaxation ($\beta \rightarrow 1$) below 240 K. Since the dielectric losses ε'' and the microwave conductivity (see next part) increase with lowering temperatures, there is a "skin effect" in the whole microwave range affecting the relaxation domain 3 below 240 K and consequently it is not possible to make measurements at lower temperatures in order to determine the β parameter. However, if we extrapolate the curve of Fig. 5 (β parameter of domain 3 = $f(T)$) toward lower temperatures the electron hopping relaxation would be of the Debye type below 220 K. This temperature value is of the same order of magnitude as that corresponding to the appearing X-ray satellite reflections ($T \approx 200$ K) in SSR single crystal bronze, which has been explained as bipolaron ordering. Assuming that the electronic properties are similar for a SSR single crystal bronze and a SGP bronze orientated film (*12*), it would be possible to correlate the non-Debye behavior ($\beta \neq 1$) with disorder below 200 K in the SGP bronze.

Frequency-Dependent Conductivity

The frequency-dependent conductivity $\sigma(\omega)$ corresponds to the real part of the complex conductivity $\sigma^*(\omega) = i\omega\,\varepsilon_0\,\varepsilon^*(\omega)$, i.e., $\sigma(\omega) = \omega\,\varepsilon_0\,\varepsilon''(\omega)$. Figure 8 shows the plots of log $\sigma(\omega)$ versus the frequency $\omega/2\pi$ for the SGP bronze in the temperature range 240–300 K.

In the low-frequency region (<20 MHz) the conductivity $\sigma(\omega)$ is almost constant and corresponds to dc or "long-range" conductivity $\sigma_{dc} \approx 4.10^{-2}$ S · cm^{-1} at 300 K (cf. Fig. 8).

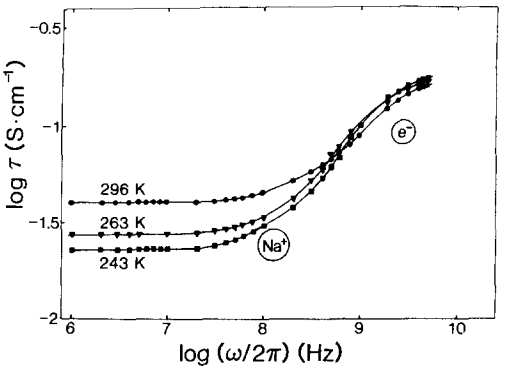

FIG. 8. Frequency-dependent conductivity $\sigma(\omega)$ of the SGP bronze along the c-axis, i.e., log $\sigma(\omega)$ vs log$(\omega/2\pi)$.

In the high frequency region, i.e., 20 MHz $< \omega/2\pi <$ 6 GHz, Fig. 8 shows a strongly frequency-dependent conductivity due to dielectric relaxations (cf. Figs. 2 and 3) corresponding to Na^+ cation hopping (several hundred MHz) and electron hopping (several GHz). In a small frequency range between 2 and 6 GHz, within the accuracy of the measurements, the conductivity becomes nearly constant. However, above 6 GHz, it was not possible to measure $\sigma(\omega)$ owing to the arising "skin effect," the penetration depth of the wave being lower than the dimensions of the sample.

Figure 9 compares the temperature dependence (log $\sigma T = f(10^3/T)$) of SGP bronze conductivity along the c-axis at low frequency (*12*) (≈ continued regime σ_{dc}) and at microwave frequency 5 GHz (σ_{mw}). Contrary to σ_{dc}, which follows an Arrhenius law with activation energy $W_c \approx 0.07$ eV, the microwave conductivity σ_{mw} is not an activated process: $\sigma_{mw}T$ is almost constant ($\sigma_{mw} \approx 45/T$) between 240 and 300 K. That may be explained if we consider the conductivity along the c-axis as being the result of electron hopping in the sequence V_1–V_3–$V_{3'}$–$V_{1'}$ (cf. Fig. 7 and Ref. (*8*)). We can deduce from these results the hopping distance corresponding to σ_{mw} in the same

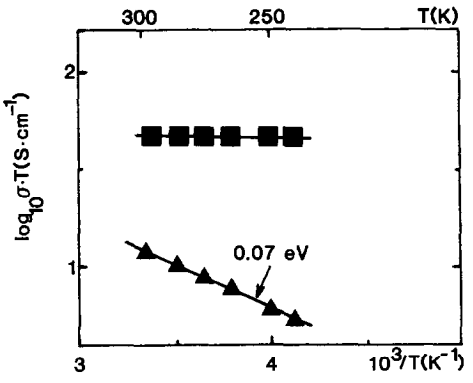

FIG. 9. Temperature dependence of the dc conductivity σ_{dc} (▲) and of the microwave conductivity σ_{mw} at 5 GHz (■) for the SGP bronze.

way as that corresponding to σ_{dc} (*11*, *12*) according to

$$\sigma_{mw}T = N_3\,[(e \cdot l_3')^2/k] \cdot \tau_0^{-1}, \qquad (5)$$

where l_3' corresponds to the hopping distance with $W = 0$ ($\exp(W/kT) = 1$) and N_3 is the concentration of single electrons expressed by Eq. (4). Assuming that $\tau_0 \approx 10^{-11}$ sec and $\Delta/k \approx 170$ K, it is found that the hopping distance $l_3' \approx 1.2$ Å. This calculated value has the same order of magnitude as the projection of the distance V_1–V_3 ($l \approx 1$ Å) on the *c*-axis, within the accuracy of the measurements.

Consequently, the microwave conductivity σ_{mw} of SGP bronze in the *ax*-plane would be due to electron local hopping between V_1 and V_3 sites (cf. Fig. 7) whose characteristic time $\tau_0 \approx 10^{-11}$ sec is not temperature dependent, in agreement with EPR study (*11*) of SSR bronze.

Conclusion

Experimental results obtained by dielectric absorption spectroscopy in the broad frequency range 1 MHz–10 GHz have shown that it is possible to observe dielectric relaxations due to Na^+ cation and electron hopping in the β-$Na_{0.33}V_2O_5$ bronze synthesized by the sol–gel process. The relaxation times and the activation energies corresponding to the hopping diffusion of charge carriers are in good agreement with those obtained by NMR and EPR techniques on a bronze single crystal synthesized by solid state reaction.

We have shown that the knowledge of the frequency-dependent conductivity $\sigma(\omega)$ of the sol–gel bronze along the *c*-axis in RF and microwave frequencies gives direct information about the charge transfer mechanisms in the time scale 10^{-6} to $10^{-11}/10^{-12}$ sec. Accordingly it is possible to discriminate between

(i) "long-range" dynamics correlated to electron hopping over several vanadium sites and corresponding to "low-frequency" or "dc" conductivity σ_{dc}, and

(ii) "local" dynamics correlated to electron hopping between neighboring vanadium sites with a correlation time $\tau_c \approx 10^{-11}$ sec and/or Na^+ cation diffusion in the tunnel sites of the oxide framework (correlation time $\tau_c \approx 5.10^{-12}$ sec). The Na^+ motion takes place in the *ac*-plane and to the hopping between available M_2 sites via equilibrium M_1 sites.

A complete description of the dynamical properties of the bronze would necessitate a similar study parallel to the film plane, i.e., essentially along the *b*-axis of the bronze, which so far could not be realized owing to a skin effect appearing in the microwave domain ($f > 300$ MHz). This study could be made with a new coaxial cell in which the sample dimensions would be lower than the penetration depth of the electromagnetic wave.

References

1. L. ZNAIDI, N. BAFFIER, AND M. HUBER, *Mater. Res. Bull.* **24**, 1501 (1989).
2. J. P. PEREIRA-RAMOS, L. ZNAIDI, N. BAFFIER, AND R. MESSINA, *Solid State Ionics*, **28–30**, 886 (1988).
3. J. GALY, M. POUCHARD, A. CASALOT, AND P.

HAGENMULLER, *Bull. Soc. Fr. Mineral. Cristallogr.* **90,** 544 (1967).
4. P. HAGENMULLER, *in* "Non-Stoichiometric Compounds, Tungsten Bronzes, Vanadium Bronzes and Related Compounds," (D. J. Bevan and P. Hagenmuller, Eds.), Vol. 1, pp. 569, Pergamon, Oxford (1973).
5. J. GALY, J. DARRIET, A. CASALOT, AND J. B. GOODENOUGH, *J. Solid State Chem.* **1,** 339 (1970).
6. J. B. GOODENOUGH, *J. Solid State Chem.* **1,** 349 (1970).
7. M. ONODA, T. TAKASHI, AND H. NAGASAWA, *Phys. Status Solidi B* **109,** 793 (1982).
8. B. K. CHAKRAVERTY, M. J. SIENKO, AND J. BONNEROT, *Phys. Rev. B* **17,** 3781 (1978).
9. J. H. PERLSTEIN AND J. SIENKO, *J. Chem. Phys.* **48,** 174 (1968).
10. V. K. KAPUSTKIN, V. L. VOLKOV, AND A. A. FOTIEV, *J. Solid State Chem.* **19,** 359 (1976).
11. H. NAGASAWA, T. ERATA, *J. Phys.* **43,** C3–C1737 (1983).
12. J. C. BADOT, D. GOURIER, F. BOURDEAU, N. BAFFIER, AND A. TABUTEAU, *J. Solid State Chem.*, in press.
13. T. ERATA AND H. NAGASAWA, *J. Phys. Soc. Jpn* **52,** 3652 (1983).
14. J. C. BADOT, A. FOURRIER-LAMER, AND N. BAFFIER, *J. Phys.* **46,** 2107 (1985).
15. H. KOLODZIEJ, L. SOBCZYK, *Acta Phys. Pol. A* **39,** 59 (1971).
16. J. C. BADOT, PhD thesis, Paris (1988).
17. W. J. GETSINGER, *IEEE Trans. Microwave Theory Tech.* **MTT-14,** 58 (1966).
18. A. CHELKOWSKI, "Dielectric Physics," Elsevier Science, New York (1980).
19. S. DATTAGUPTA, "Relaxation Phenomena in Condensed Matter Physics," Academic Press, San Diego (1987).
20. N. KUMAR, *in* "Non-Debye Relaxation in Condensed Matter, Proceedings of a Discussion Meeting, Bangalore," (T. V. Ramakrishnan and M. Raj Lakshmi, Eds.), p. 11, World Scientific (1987).
21. T. V. RAMAKRISHNAN, *in* "Non Debye Relaxation in Condensed Matter, Proceedings of a Discussion Meeting Bangalore," (T. V. Ramakrishnan and M. Raj Lakshmi, Eds.), p. 2, World Scientific (1987).